



Size modulation of nanocrystalline silicon embedded in amorphous silicon oxide by Cat-CVD

Y. Matsumoto^{a,b,*}, S. Godavarthi^b, M. Ortega^{a,b}, V. Sánchez^a, S. Velumani^{a,b}, P.S. Mallick^c

^a Electrical Engineering Department, Centro de Investigación y de Estudios Avanzados del IPN, Av. IPN 2508, Col. San Pedro Zacatenco, Mexico City 07360, Mexico

^b Program of Nanoscience and Nanotechnology, Centro de Investigación y de Estudios Avanzados del IPN, Av. IPN 2508, Col. San Pedro Zacatenco, Mexico City 07360, Mexico

^c School of Electrical Sciences, Center for Nanotechnology, VIT University, Vellore, India

ARTICLE INFO

Available online 25 February 2011

Keywords:

Nanocrystalline-silicon

Cat-CVD

X-ray-diffraction

Micro-Raman

ABSTRACT

Different issues related to controlling size of nanocrystalline silicon (nc-Si) embedded in hydrogenated amorphous silicon oxide (a-SiO_x:H) deposited by catalytic chemical vapor deposition (Cat-CVD) have been reported. Films were deposited using tantalum (Ta) and tungsten (W) filaments and it is observed that films deposited using tantalum filament resulted in good control on the properties. The parameters which can affect the size of nc-Si domains have been studied which include hydrogen flow rate, catalyst and substrate temperatures. The deposited samples are characterized by X-ray diffraction, HRTEM and micro-Raman spectroscopy, for determining the size of the deposited nc-Si. The crystallite formation starts for Ta-catalyst around the temperature of 1700 °C.

© 2011 Elsevier B.V. All rights reserved.

1. Introduction

Different types of thin film silicon materials like amorphous (a-Si:H) [1], protocrystalline (pr-Si:H) [2], polymorphous (pm-Si:H) [3], nanocrystalline (nc-Si) [4], microcrystalline (μc-Si:H) [5] and polycrystalline silicon (poly-Si:H) [6] have been developed for several applications. At first sight, the different morphologies could be generally classified by the differences in the amount of amorphous phase present and the crystallite size. The term nc-Si embedded in a-SiO_x:H refers to a range of materials around the transition region from amorphous to microcrystalline phase. nc-Si offers several advantages compared to a-Si:H, which makes it an ideal material for the future generation PV devices. It is already reported [7] that nc-Si does not show the light induced degradation which has been the limiting factor for expansion of a-Si:H.

A great number of techniques can be used to produce nc-Si embedded in a-Si:H, such as sputtering [8–11], ion implantation [12–14] plasma enhanced chemical vapor deposition (PE-CVD) [15,16], low-pressure CVD (LPCVD) [17], pulsed laser deposition (PLD) [18,19], and catalytic-CVD (cat-CVD) [20]. We have chosen the widely accepted technique cat-CVD due to our interest in controlling the crystallites size. Hence the present work is divided into two parts a) to determine the catalyst W or Ta and b) controlled deposition of nc-Si embedded in a-SiO_x:H by using Ta catalyst. The deposited films, as a function of hydrogen flow, catalyst and substrate temperatures, were characterized by X-ray diffraction (XRD) and micro Raman for determining its crystallite sizes.

2. Experimental

The cat-CVD system has been already described elsewhere [21]. The distance between the catalyst and sample, gas inlets and catalyst, was set at 5 cm. The shape of the filament was single coiled type has been used for all the depositions. We deposited films on glass substrates and c-Si substrates. The glass substrates are of Corning 2947 C and of 1.1 mm thickness and c-Si are of Boron doped p-type and of 525 μm thickness. Previous to the film formation, the substrates have cleaned from organic and metal impurities by using the conventional RCA method [22]. Upon creating high vacuum of 10⁻⁶ Torr, chamber was backfilled by reactive gasses and kept at 0.1 Torr for deposition.

2.1. Determination of catalyst material

Oxygen-rich boron-doped hydrogenated nanocrystallite silicon films were deposited using Ta and W catalysts. Ta and W catalysts were heated from 1800 to 1950 °C and substrates temperature (T_{sub}) is maintained at 200 °C. Silane (SiH₄), diborate (B₂H₆), Hydrogen (H₂) and Oxygen (O₂) gasses with flow rates 5, 10, 5 and 5 standard cubic centimeter per minute (sccm), respectively, were introduced into the process chamber.

2.2. Deposition of nc-Si

SiH₄, O₂ and H₂ gasses were used for the nc-Si deposition. The SiH₄ and O₂ flow rates were kept constant at 5 sccm. The depositions were carried at different catalyst temperatures (T_{fil}), substrate temperatures (T_{sub}) and H₂ flow ratio. The T_{fil} varied from 1700 to 1950 °C in steps of 50 °C. The T_{sub} was varied from 150 to 250 °C in steps of 50 °C.

* Corresponding author.

E-mail address: [ymatsumo@cinvestav.mx](mailto:yamatsumo@cinvestav.mx) (Y. Matsumoto).

The thickness of the deposited films is around 300 nm measured by Tenkor P15 profilometer.

The deposited films are analyzed by XRD using Siemens D5000 and grain size was determined using Scherrer formula [23]. For Raman Spectroscopy, spectrometer Jobin-Yvon T64000 with a laser beam at a wavelength of 514 cm^{-1} was used. The characteristic peak corresponding to the transverse optical mode of crystalline silicon can be found at 520 cm^{-1} , whereas the amorphous band appears around 480 cm^{-1} . The mean size of the nanocrystallites can be found using formula [24]

$$d = 2\pi \left(\frac{B}{\Delta\omega} \right)^{1/2} \quad (1)$$

Where d = size of the nanocrystallites, $\Delta\omega$ = peak shift for the nanocrystalline as compared that of the c-Si, $B = 2.0\text{ nm}^2\text{ cm}^{-1}$.

3. Results and discussions

3.1. Optimization of catalyst

Fig. 1 shows conductivity as a function of the catalyst temperature. The measured deposition rate (d_r) obtained from thickness using profilometer were $0.40\text{--}0.54\text{ nm/s}$ for both Ta and W. The measured dark-conductivity (σ) for Ta has varied from $7.0 \times 10^{-8}\text{--}2.0 \times 10^{-5}\ \Omega^{-1}\text{ cm}^{-1}$. In comparison to Ta, W catalyst has achieved higher σ of $5.0 \times 10^{-3}\ \Omega^{-1}\text{ cm}^{-1}$ with similar d_r as Ta. The σ increment at higher T_{fil} , is explained by the nanocrystalline phase formation demonstrated by XRD spectra shown in the inset of Fig. 1 (only for W) [25]. For the samples prepared using Ta catalyst, the amorphous to nanocrystalline phase transition occurs gradually within the temperature range of 1800 to $1950\text{ }^\circ\text{C}$. But the samples prepared using W catalyst showed abrupt transition in the same T_{fil} range.

The so-called *temperature-activated conductivity-transition* properties of amorphous to nanocrystalline-phases seem to be different between Ta and W. This happens due to the silicon content in the near surface region of the filament, which is called silicidation, and is larger in the case of a tungsten filament as compared to tantalum filament. Hence, the catalytic dissociation of the reactant gasses may be different for tantalum compared to tungsten surface [26], which may provide different crystalline growth kinetics in the case of tantalum. Therefore, it is concluded that tantalum catalyst yielded better controllability over

amorphous to nc-Si transition compared to W catalyst, and remaining experiments were carried out using Ta catalyst.

3.2. Deposition of nc-Si

Figs. 2 to 4 show XRD patterns of deposited samples. Three main peaks are observed in several samples. The peak at 28.4° , 47.3° and 56.1° are corresponding to the Si (111), (220) and (311) planes respectively. One more peak at 25.6° was observed for films deposited above $1800\text{ }^\circ\text{C}$. The mentioned peak may belong to SiO_x -related phase [27], and the broad area under the Si (111) peak, could be due to the glass substrate component which indicates its amorphous structure.

3.2.1. The role of catalyst temperature

Fig. 2(a) shows XRD pattern of the films with increasing catalyst temperature (bottom to top) at $T_{sub} = 200\text{ }^\circ\text{C}$ and $\text{SiH}_4/\text{O}_2/\text{H}_2 = 5/5/10$. At $T_{fil} = 1700\text{ }^\circ\text{C}$ a broad peak without any orientation is observed but at $T_{fil} = 1750\text{ }^\circ\text{C}$ a clear (111) crystalline plane is formed. Hence it is clear that catalyst temperature plays an important role in promoting the nanocrystallite structure. Fig. 2(b) shows nc-Si formation tendency with increasing the catalyst temperature (bottom to top) for $T_{sub} = 200\text{ }^\circ\text{C}$ and $\text{SiH}_4/\text{O}_2/\text{H}_2 = 5/5/15$. The corresponding average crystallite sizes are given in Table 1. From Fig. 2(b) and Table 1, no crystallite formations

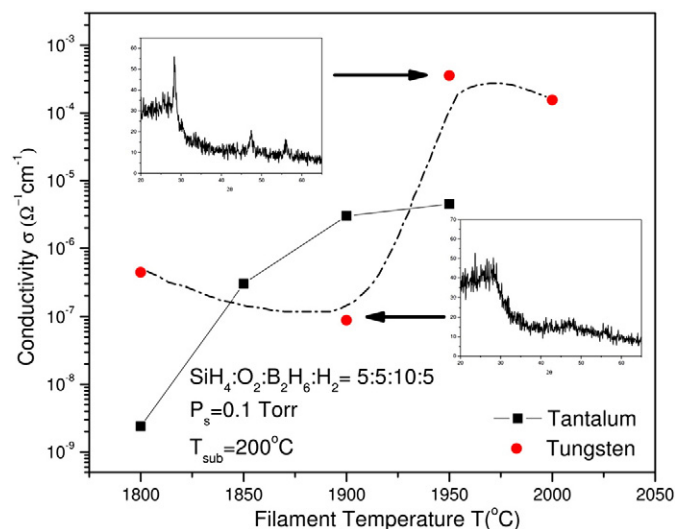


Fig. 1. Conductivity of nanocrystalline Silicon deposited with W and Ta filaments as a function of filament temperature. Inset figure, indicates XRD spectra for amorphous and nanocrystallite phases for W.

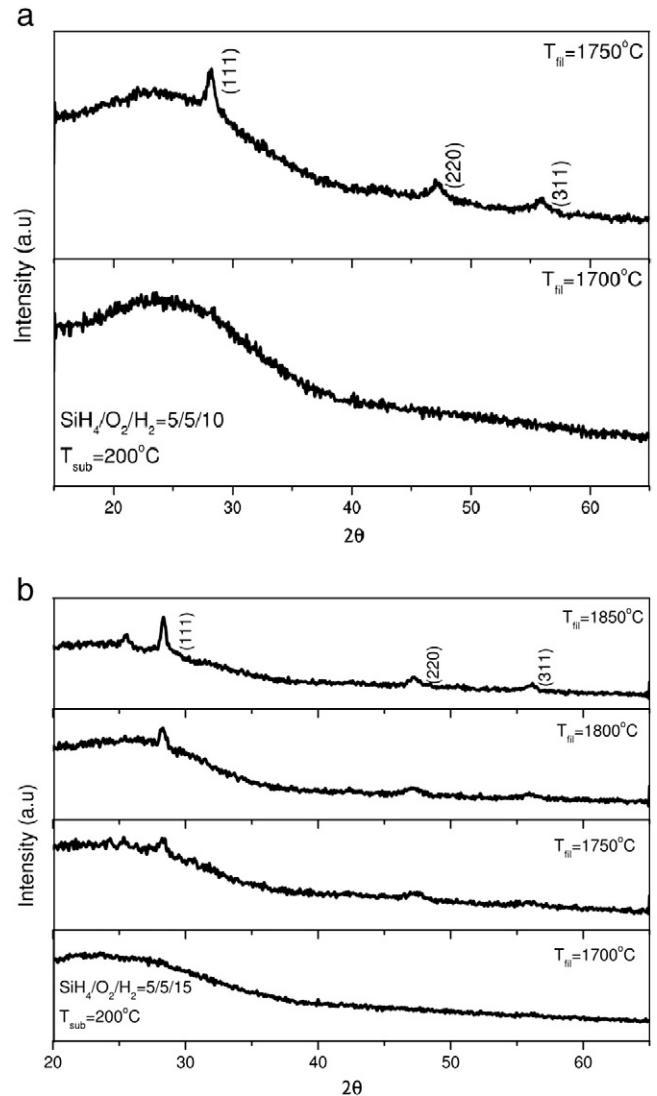


Fig. 2. (a) XRD spectra for sample prepared at different catalyst temperature with: $T_{sub} = 200\text{ }^\circ\text{C}$ and $\text{SiH}_4/\text{O}_2/\text{H}_2 = 5/5/10$, (b) $\text{SiH}_4/\text{O}_2/\text{H}_2 = 5/5/15$.

are apparent at $T_{fil}=1700\text{ }^{\circ}\text{C}$ i.e. the deposited film remains in amorphous phase. However, the crystallites start growing at $T_{fil}=1750\text{ }^{\circ}\text{C}$ and the size of the crystallite increases with the catalyst temperature. The formation of the nc-Si phases is related to the differences in the dissociated amount of hydrogen that depends on temperature-related energy at the filament. At low filament temperature there will be less amount of available atomic hydrogen which is considered as more important for etching weak bonds i.e. amorphous phased dangling bonds during the film growth. The availability of atomic hydrogen increases with increases of filament temperature, hence, helps the crystallites formation and growth [28].

3.2.2. The role of substrate temperature

Fig. 3(a) shows the XRD spectra for samples prepared at different substrate temperatures of 150, 200 and 250 $^{\circ}\text{C}$ with fixed $T_{fil}=1700\text{ }^{\circ}\text{C}$ and $\text{SiH}_4/\text{O}_2/\text{H}_2=5/5/15$. The deposited films are in amorphous phase for samples prepared at $T_{sub}=150$ and 200 $^{\circ}\text{C}$. But, at $T_{sub}=250\text{ }^{\circ}\text{C}$, the crystallites start growing and found that the average size is below 10 nm. The substrate temperature effect could be explained as follow. At low substrate temperatures, deposited atoms, molecules or radicals are not in positions to diffuse and to accommodate themselves to form a crystalline-involved structure, because of low energy. However, with increasing the substrate temperature, the energy possessing by these radicals will increase. They can diffuse on the surface so that they can accommodate themselves to form crystallites.

When compared Fig. 3(b) with Fig. 3(a) in spite of lower hydrogen flow of 5 sccm, the sample prepared at $T_{sub}=200\text{ }^{\circ}\text{C}$ starts promoting crystallite formation. From the present results, the substrate temperature has an important contribution for crystallites formation. The calculated average nc-Si sizes are around 6–8 nm using Scherrer's formula. Fig. 3(c) shows the Raman spectra of the nc-Si films deposited, for which deposition conditions are corresponding to the samples given in Fig. 3(b). The film with substrate temperatures of 150 $^{\circ}\text{C}$ exhibits Raman peak at 480 cm^{-1} , showing amorphous phase. But films with $T_{sub}=200\text{ }^{\circ}\text{C}$ and 250 $^{\circ}\text{C}$ exhibited peaks at 518.02 cm^{-1} , showing the nc-Si phases. After substituting the peak shift in Eq. (1) the deviation in the crystallite size about 25% was observed when compared with the XRD result. The differences in the crystallite sizes between XRD and Raman analysis can be explained as a strain present in the film. If the films are strained due to oxidation or some other means, peak will be shifted towards lower frequency side [29]. Hence results small crystallite sizes in Raman analysis.

3.2.3. The role of hydrogen flow rate

Fig. 4 shows the crystalline formation process as a function of hydrogen dilution for $T_{fil}=1700\text{ }^{\circ}\text{C}$ and $T_{sub}=250\text{ }^{\circ}\text{C}$. It is observed that no crystallinity was observed at 5 sccm of hydrogen flow. However, at 15 sccm a formation of nanocrystallites was found. The average nanocrystallites size is around 8.7 nm using Scherrer's formula. It is clear that hydrogen helps the crystallites formation. By increasing the hydrogen dilution ratio in the chamber, we increase the relative amount between atomic hydrogen and silicon. This results in more etching of weak bonds during film growth, resulting in more crystalline films [28,30].

In the present case, the entire growth mechanism for the nc-Si material, has to be considered with the interaction of oxygen molecules, i.e. the formation of a-SiO_x:H. Conventionally the nc-Si nucleation occurs starting at the a-Si:H phases [31], but in the present circumstances, oxygen molecules may act also as an Si–Si formation inhibitor.

3.3. High resolution transmission electron microscopy (HRTEM)

Alternatively in Fig. 5 shows high-resolution transmission electron microscopy (HRTEM) Jeol JSM 2010F for the nc-Si deposited at

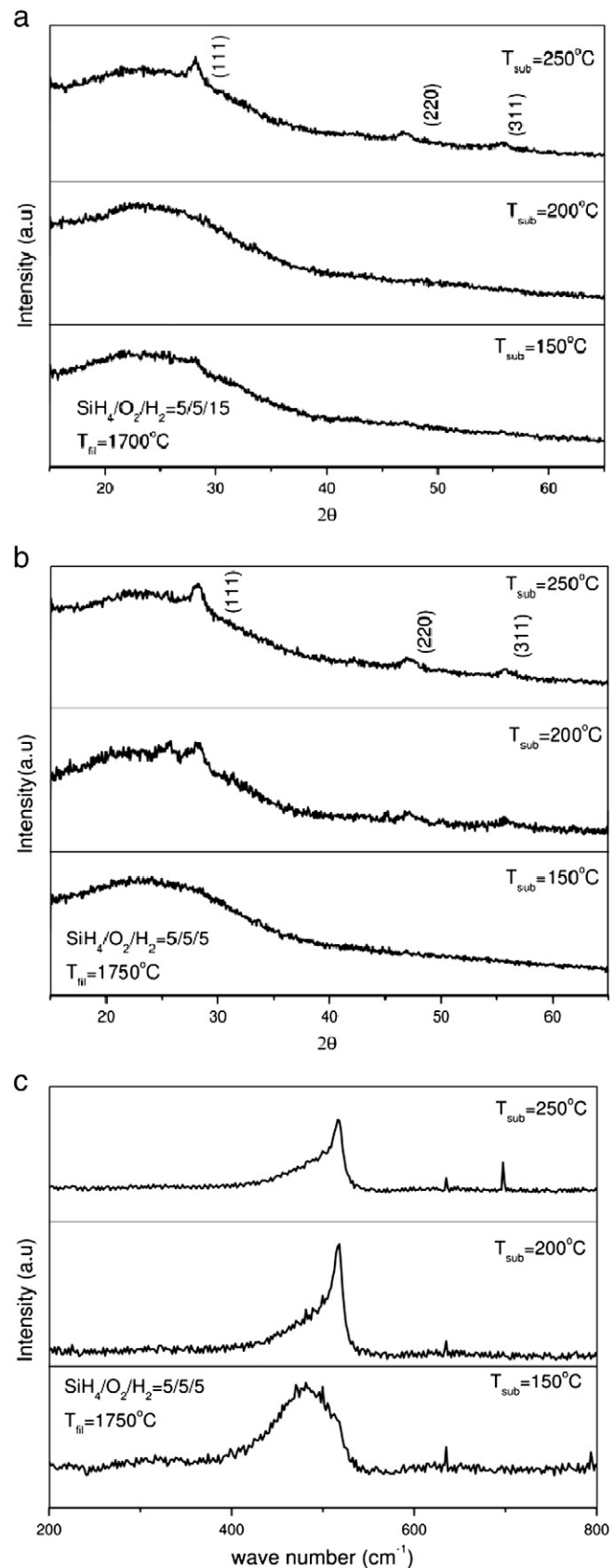


Fig. 3. (a) XRD spectra for the samples deposited at different substrate temperatures with: $T_{fil}=1700\text{ }^{\circ}\text{C}$ and $\text{SiH}_4/\text{O}_2/\text{H}_2=5/5/15$. (b) $T_{fil}=1750\text{ }^{\circ}\text{C}$ and $\text{SiH}_4/\text{O}_2/\text{H}_2=5/5/5$. (c) Raman spectra for samples with different T_{sub} at $T_{fil}=1750\text{ }^{\circ}\text{C}$, $\text{SiH}_4/\text{O}_2/\text{H}_2=5/5/5$, for the same samples shown in Fig. 3(b).

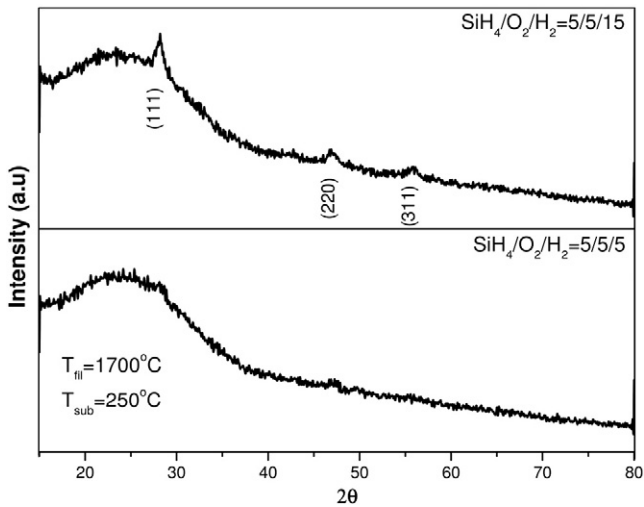


Fig. 4. XRD spectra for the samples deposited at different hydrogen flow at $T_{fil} = 1700\text{ °C}$ and $T_{sub} = 250\text{ °C}$, with constant $\text{SiH}_4/\text{O}_2 = 5/5$ flow.

Table 1

Crystallite size variation as a function of the catalyst temperature for $\text{SiH}_4/\text{O}_2/\text{H}_2 = 5/5/15$, $T_{sub} = 200\text{ °C}$, as samples of Fig. 3(a).

Catalyst temp.	(111) (nm)	(220) (nm)	(311) (nm)	Average (nm)
1700 °C	–	–	–	–
1750 °C	15.3	7.7	–	7.6
1800 °C	13.8	6.1	6.8	8.9
1850 °C	19.8	8.6	12.7	13.7

$T_{sub} = 200\text{ °C}$, $\text{SiH}_4/\text{O}_2/\text{H}_2 = 5/5/5$ and $T_{fil} = 1750\text{ °C}$, the approximate crystallite size is 7 to 9 nm which is consistent with the XRD result.

4. Conclusion

nc-Si embedded in an a-SiO_x:H films were deposited using Ta catalyst using Cat-CVD process. Between the W and Ta catalysts, the tantalum had better amorphous to nanocrystallite phase-transition controllability to form nc-Si embedded in an a-SiO_x:H films.

The nc-Si was observed at T_{fil} as low as 1700 °C, however, the lowest crystallite size 7.6 nm was found at $T_{fil} = 1750\text{ °C}$; $T_{sub} = 200\text{ °C}$ and $\text{SiH}_4/\text{O}_2/\text{H}_2 = 5/5/15$. It is observed that the crystallite size is easily growing with increase of catalyst temperature with fixed T_{sub} and H_2 flow rate. It is observed that at $T_{fil} = 1750\text{ °C}$ and above, the crystallite size grows with increase of T_{sub} with irrespective of H_2 flow rate. It is observed that increasing the H_2 flow, decreases the deposition rate. This results from etching of dangling bonds. This effect is important in the formation of nc-Si. The measured grain values of nc-Si using Raman spectra are deviating from those of XRD. This is explained by considering the strain present in the film.

Acknowledgment

The authors thank Angela Gabriela López for sample preparations. The authors are indebted to Miguel Angel Luna for sample thickness measurements, Marcela Guerrero and Alejandra García of Physics Department for XRD and Raman measurements, respectively. Also the authors are indebted to Dr. Jesus A. Arenas of IF-UNAM, Physics Institute of the National Autonomous University for HRTEM measurements.

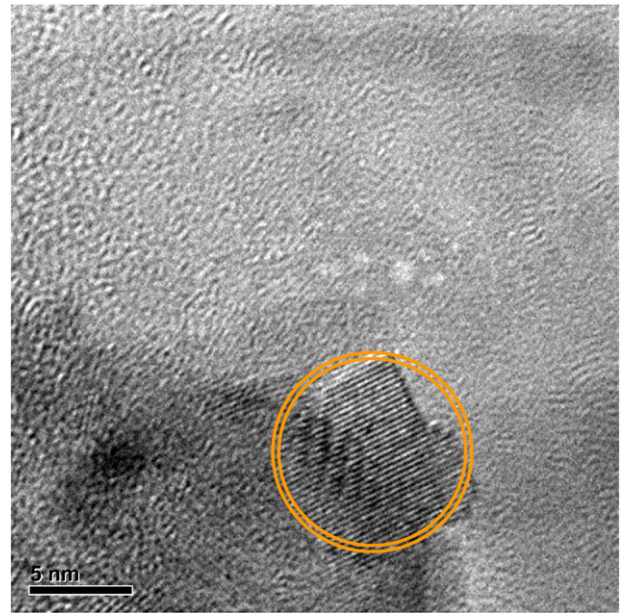


Fig. 5. High-resolution transmission electron microscopy (HRTEM) for the nc-Si deposited at $T_{sub} = 200\text{ °C}$, $\text{SiH}_4/\text{O}_2/\text{H}_2 = 5/5/15$ and $T_{fil} = 1700\text{ °C}$.

References

- [1] H. Shanks, C.J. Fang, L. Ley, M. Cardona, F.J. Demond, S. Kalbitzer, *Phys. Status Solidi B* 100 (1980) 43.
- [2] J. Koh, A.S. Ferlauto, P.I. Rovira, C.R. Wronski, R.W. Collins, *Appl. Phys. Lett.* 75 (1999) 2286.
- [3] A. Fontcuberta, H. Hfmeister, P. Roca, *J. Non-Cryst. Solids* 299–302 (2002) 284.
- [4] Nobuyasu Suzuki, Toshiharu Makino, Yuka Yamada, Takehito Yoshida, *Appl. Phys. Lett.* 76 (2000) 1389.
- [5] J. Meier, et al., *Sol. Energy Mater. Sol. Cells* 49 (1997) 35.
- [6] R.E.I. Schropp, J.K. Rath, *IEEE Trans. Electron Dev.* 46 (10) (1999) 2069.
- [7] V. Shah, J. Meier, E. Vallat-Sauvain, N. Wyrshch, U. Kroll, C. Droz, U. Graf, *Sol. Energy Mater. Sol. Cells* 78 (2003) 469.
- [8] Y. Kanzawa, *Solid State Commun.* 02 (1997) 533.
- [9] L. Tsybeskov, *Appl. Phys. Lett.* 72 (1998) 43.
- [10] S. Charvet, R. Madelon, R. Rizk, *Solid State Electron.* 45 (2001) 1505.
- [11] T.V. Torchynska, M.M. Rodriguez, Y. Golstein, A. Many, E. Endzewski, B.M. Bulakh, L.V. Scherbina, *Phys. B* 308–310 (2001) 948.
- [12] B. Garrido, M. Lopez, S. Ferre, A. Romato-Rodriguez, A. Perez-Rodriguez, P. Ruterana, J.R. Morante, *Nucl. Instrum. Meth. B* 120 (1996) 101.
- [13] H.Z. song, X.M. Bao, *Phys. Rev. B* 55 (997) 6988.
- [14] S. Chelan, R.G. Elliman, *Appl. Phys. Lett.* 78 (2001) 1912.
- [15] G. Franzo, F. Iacona, C. Spinella, S. Cammarata, M.G. Grimaldi, *Mater. Sci. Eng. B* 69 (70) (2002) 454.
- [16] T. Inokuma, Y. Wakayama, T. Muramoto, R. Aoki, Y. Kurata, S. Hasegawa, *J. Appl. Phys.* 83 (1998) 2228.
- [17] A. Morales, J. Barreto, C. Dominguez, M. Riera, M. Aceves, J. Carrillo, *Phys. E* 38 (2007) 54.
- [18] Jong Hoon Kim, *Opt. Mater.* 27 (2005) 991.
- [19] N. Suzuki, T. Makino, Y. Yamada, T. Yoshida, *Appl. Phys. Lett.* 76 (11) (2000) 1389.
- [20] T.V. Torchynska, A. Vivas Hernandez, M. Dybiec, Yu. Emirov, I. Tarasov, S. Ostapenko, Y. Matsumoto, *Phys. Stat. Sol. B* (2005) 1832.
- [21] Y. Matsumoto, *Thin Solid Films* 501 (2006) 95.
- [22] W.A. Kern, D.A. Poutinen, *RCA Rev* 31 (1970) 187.
- [23] B.D. Cullity, 2nd ed, Addison-Wesley, Reading, MA, 1978, p. 284.
- [24] He Yuilang, Yin Chenzhong, Guangxuxu cheng, Wang Luchun, xiangna Liu, *J. Appl. Phys.* 75 (2) (1994) 797.
- [25] Y. Matsumoto, Z. Yu, V. Sanchez, *Sol. Energy Mater. Sol. Cells* 92 (2008) 576.
- [26] P.A.T.T. van Veenendaal, O.L.J. Gijzeman, J.K. Rath, R.E.I. Schropp, *Thin Solid Films* 395 (2001) 194.
- [27] Raul F. Lobo, Mark E. Davis, *J. Am. Chem. Soc.* 117 (1995) 3766.
- [28] H.R. Moutinho, C.-S. Jiang, Y. Xu, B. To, K.M. Jones, C.W. Teplin, M.M. Al-Jassim, <http://www.nrel.gov/docs/fy05osti/37345.pdf>.
- [29] O. Marty, T. Nychporuk, J. de la Torre, V. Lysenko, a. G. Bremond, D. Barbier, *Appl. Phys. Lett.* 88 (2006) 101909.
- [30] R. Banerjee, S.N. Sharma, A.K. Bandyopadhyay, A.K. Batabyal, A.K. Barua, *J. Mater. Sci. Lett.* 12 (1993) 1316.
- [31] H. Fujiwara, M. Kondo, A. Matsuda, *Jpn. J. Appl. Phys.* 41 (2002) 2821.